



City Research Online

City, University of London Institutional Repository

Citation: Syamil Mohd Sa'ad, M., Faizal Ismail, M., Khairol Annuar Zaini, M., Grattan, K. T. V., Rahman, B. M., Brambilla, G., Sing, L. K. & Ahmad, H. (2022). Temperature-independent Vibration Sensor Based on Fabry-Perot Interferometer using a Fiber Bragg Grating approach. *Optical Engineering*, 61(03), 037101. doi: 10.1117/1.oe.61.3.037101

This is the accepted version of the paper.

This version of the publication may differ from the final published version.

Permanent repository link: <https://openaccess.city.ac.uk/id/eprint/27741/>

Link to published version: <https://doi.org/10.1117/1.oe.61.3.037101>

Copyright: City Research Online aims to make research outputs of City, University of London available to a wider audience. Copyright and Moral Rights remain with the author(s) and/or copyright holders. URLs from City Research Online may be freely distributed and linked to.

Reuse: Copies of full items can be used for personal research or study, educational, or not-for-profit purposes without prior permission or charge. Provided that the authors, title and full bibliographic details are credited, a hyperlink and/or URL is given for the original metadata page and the content is not changed in any way.

City Research Online:

<http://openaccess.city.ac.uk/>

publications@city.ac.uk

Temperature-independent vibration sensor based on Fabry–Perot interferometer using a fiber Bragg grating approach

Muhammad Syamil Mohd Sa'ad^{1b},^a Mohammad Faizal Ismail,^a
Muhammad Khairol Annuar Zaini^{1b},^a Kenneth T. V. Grattan^{1b},^b
B. M. Azizur Rahman,^b Gilberto Brambilla,^c Lim Kok Sing^{1b},^a
and Harith Ahmad^{a,d,e}

^aUniversiti Malaya, Photonics Research Center, Kuala Lumpur, Malaysia

^bCity University of London, School of Mathematics, Computer Science and Engineering,
London, United Kingdom

^cUniversity of Southampton, Optoelectronics Research Centre, Southampton, United Kingdom

^dUniversiti Malaya, Physics Department, Faculty of Science, Kuala Lumpur, Malaysia

^eAirlangga University, Department of Physics, Faculty of Science and Technology,
Surabaya, Indonesia

Abstract. An innovative vibration sensor based on a Fabry–Perot interferometer (FPI) using fiber Bragg grating (FBG) reflectors was demonstrated in this work. The sensor was designed to be compact and easy to fabricate, independent of temperature, to overcome limitations seen in previous designs, providing an effective correction for temperature effects in FBG-based FPI (FBG-FPI) sensors. A laser source with a peak wavelength of 1547.42 nm obtained from the FBG reflective peak was used to illuminate the FBG-FPI so that the light source was always within the FBG-FPI optimum wavelength operating range of 1547.15 to 1547.80 nm. The sensor was shown to capture a 3-kHz burst signal from a signal generator in 1-, 2-, and 3-Hz intervals. In addition, the work carried out has revealed that the sensor could be used to capture sinusoidal signals at frequencies up to 9 kHz, creating a performance comparable with many existing conventional piezoelectric sensors. Furthermore, the ability to operate regardless of any ambient temperature changes [from 26.5°C (room temperature) up to 80°C] opens the way to use such a sensor system over a wide range of engineering applications taking advantage of the next generation of FBG-based FPIs.

Keywords: Fabry–Perot interferometer; fiber Bragg gratings; vibration sensor; temperature-independent.

1 Introduction

Vibration measurement is of critical concern in many current engineering applications. For example, excessive vibration or vibration at particular frequencies can have a series of effects on the performance and safety of many engineering structures, such as aircraft or buildings. Hence, accurate measurement and monitoring must be done precisely and efficiently to detect anomalous events and warn of potential infrastructure damage.¹ Vibration sensors based on piezoelectric,^{2,3} magnetostrictive,⁴ capacitive,⁵ and inductive⁶ technologies, among others, are already available and widely used by engineers in the industry. However, there are problems for many critical applications—traditional vibration sensors suffer from electromagnetic (EM) interference, making them unsuitable when applied to many challenging situations. In addition, electrical sensors may be inappropriate for use in some safety-critical regions, e.g., where explosive or flammable gases are present. Furthermore, with the developing needs in modern

engineering measurement, there is a requirement for new designs that can overcome limitations experienced in some applications (e.g., civil infrastructure) and the expensive maintenance costs required for some designs of sensor systems.

Optical fiber-based systems offer new opportunities for better sensor design, and these have received significant attention in research to address a wide range of applications over the last several decades, taking advantage of their being lightweight, operational over considerable lengths (through multiplexing of the sensors along with the optical network), potentially high accuracy, having good signal transmission security and due to their configuration, relatively easy installation, as well as corrosion resistance (not being metallic) and immunity to EM interference.^{7,8} These features emphasize their potential to be used in harsh environments⁹ where conventional sensors are often limited. Building on the low cost of many fiber optic components (due to their widespread use in telecommunications), these are well suited to many different areas of optical fiber sensing, with key examples already proven to be strain sensors,^{10–12} temperature sensors,^{13,14} and vibration sensors,^{15,16} often showing high sensitivity.¹⁷

A fiber-optic vibration sensor can typically be based on the modulation of the light properties in the optical fiber, such as intensity, phase, polarization state, and frequency, where these are (mainly) caused by externally applied vibration (and compensation for extraneous effects such as temperature can be included). The most common fiber-optic vibration sensors discussed in the literature are point,^{18–21} quasi-distributed,²² and distributed sensors.^{23,24} Different (and often complementary) optical techniques can be employed for each of these. For vibration measurement, several point sensor schemes, such as fiber Bragg gratings (FBGs), Fabry–Pérot interferometers,^{25,26} self-mixing of optical signals,²⁷ and Doppler vibrometry^{28,29} have been reported in the literature. Furthermore, because of inherent features of the optically based technique such as low noise, ease of being embedded in a structure, and the ability to be multiplexed to form a quasi-distributed sensor array, FBG vibration sensors have become a rapidly growing scientific research topic^{30,31} to meet the range of new engineering applications, both current and under development, where better vibration measurement is needed.

Among the wide range of FBG-based sensors that have already been proposed, relatively few FBG-based Fabry–Pérot interferometer (FPI) sensors have been discussed in the literature.^{32–35} Among these, Wada et al.^{32,33} used a tunable laser diode to illuminate the FBG-FPI sensor, subjected to a sinusoidal vibration. In addition, Zaini et al.³⁵ have used an edge filter interrogation method, where a further FBG-FPI was included to filter the output signal from the FBG-FPI used as the sensor. In these designs,^{32,33,35} while an effective FBG-FPI-based vibration sensor has been developed, but without an explicit temperature compensation scheme. Rao et al.³⁴ have discussed an FBG-FPI-based design to simultaneously monitor strain, temperature, and vibration. Although in that work, the FBG-based sensor was used from room temperature to 50°C, temperature effects were not eliminated when making vibration measurements using this FBG-based approach.

This work developed a temperature-independent vibration sensor using an FPI approach that is based on FBG technology to overcome the current limitations. This new sensor approach can detect burst signals at low frequencies and can find applications in areas such as ground/slope monitoring and structural vibrations as in structural health monitoring (SHM). The target performance specification of the sensor design proposed was to detect a ~3 kHz burst at 1, 2, and 3 Hz frequencies, doing so over a range of temperatures while eliminating any temperature effects. Furthermore, the results obtained have shown that the sensor can monitor sinusoidal signals, at frequencies up to ~9 kHz, independent of temperature in the detection of low-frequency burst signals and high-frequency sinusoidal waves, in this way creating a sensor scheme that potentially addressed critical sensing needs for the next generation of FBG-based FPI devices.

2 Methodology

2.1 Fabrication of the Fiber Bragg Gratings

The FBGs used in this study were fabricated by inscribing uniform gratings in conventional single-mode fiber (SMF) core, using the phase mask technique. Before this, the optical fiber

was sensitized by hydrogen-loading the SMF used for 5 days in a high-pressure hydrogen chamber. Following that, the gratings were inscribed at a length of ~ 10 -mm inside the fiber core using a Krypton fluoride (KrF*) excimer laser, operating at a wavelength of 248 nm. Finally, the fiber samples containing the inscribed gratings were heated in an oven at 70°C to 80°C for about 7 h to remove any remaining hydrogen present and stabilize the gratings.

For every FBG inscribed in an SMF, the shift of the Bragg wavelength can be linearly related with the change of strain, ε , and temperature, T , as described by the following relationship:

$$\frac{\Delta\lambda_B}{\lambda_B} = (1 - p_{\text{eff}})\Delta\varepsilon + (\alpha + \xi)\Delta T, \quad (1)$$

where λ_B represent the Bragg wavelength, while p_{eff} , α , and ξ are for the photo-elastic parameter, thermal expansion coefficient, and thermo-optic coefficient of the fiber, respectively.

2.2 Fabrication of In-Fiber FPI

In a way similar to the fabrication of the FBGs themselves, the in-fiber FPI was formed by using two identical gratings, forming extremely narrow fringes that were linearly shifted with the change of temperature and strain applied to the FBG-FPI. The FBG-FPI was formed by two short uniform gratings, as shown in Fig. 1, where in this case, the gratings of equal lengths (L_{FBG}) of 2 mm were separated by a length of 15 mm, L_{FPI} , to produce the interferometric spectra. Figure 2(a) shows the reflection spectra of an individual grating reflector (a single grating FBG, operating at 1547.42 nm). The bare fiber between the two grating reflectors creates the cavity for the resonating optical wave between the two reflectors, producing the interferometric output spectra, as shown in Fig. 2(b).

2.3 Experimental Design

The experimental setup used is shown in Fig. 3(a), where two types of the sensor were used, the first being a normal FBG with a reflection peak wavelength of 1547.42 nm, while the second was an FBG-based FPI (denoted as FBG-FPI) with an optimum operating wavelength range of

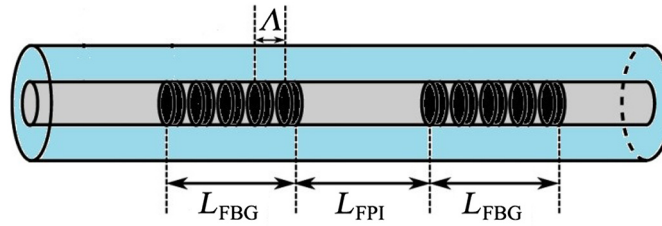


Fig. 1 Illustration of the FBG-FPI fabricated in this work where L_{FBG} is the length of the grating used (of period Λ) and L_{FPI} is the separation of the gratings, and thus the interferometric cavity length.

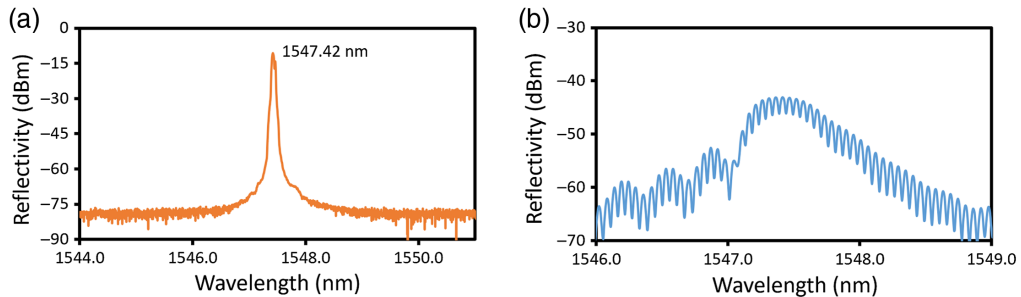


Fig. 2 Illustrations of (a) a single FBG spectrum of wavelength 1547.42 nm and (b) a typical spectrum of the FBG-FPI.

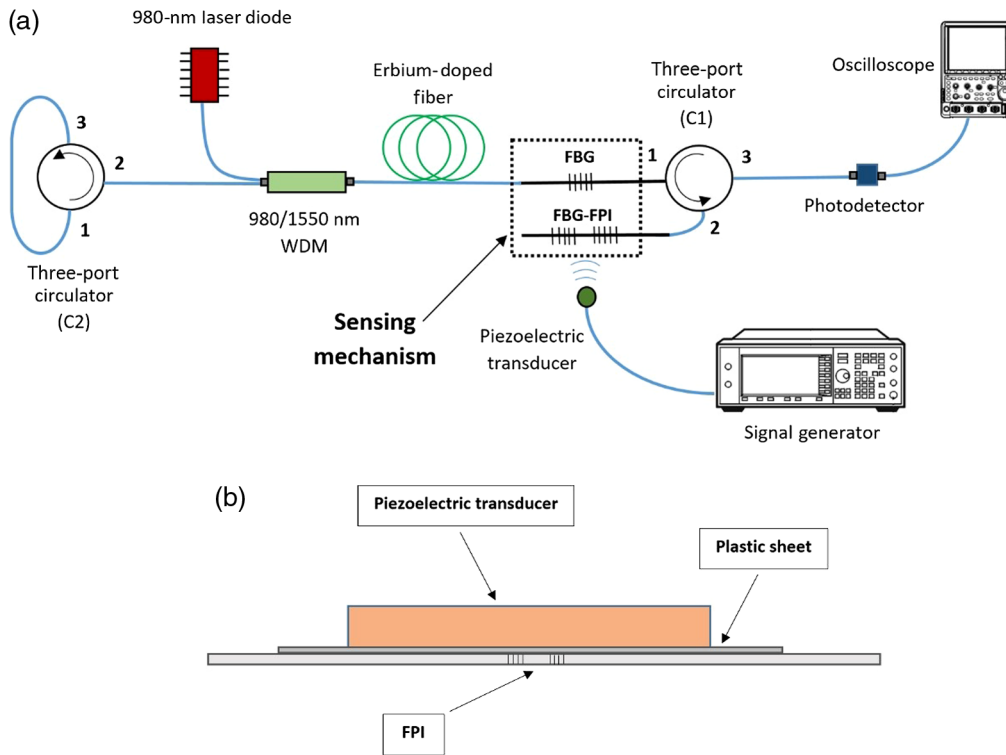


Fig. 3 Illustration of the (a) experimental setup for verifying the performance of the FBG-FPI cavity subjected to a simulated seismic-induced vibration and (b) a closer look from the side view of the signal transfer setup at the FBG-FPI.

1547.15 to 1547.80 nm. Both FBG and FBG-FPI have a reflectivity value of 80%. A 980-nm laser diode was used to pump a 0.3-m erbium-doped fiber through a 980/1550 nm wavelength division multiplexer (WDM) to produce a broad amplified spontaneous emission (ASE) over the range of 1520 to 1570 nm. This emission passes through the FBG connected to the port 1 of a three-port optical circulator (C1). The signal at the FBG reflective wavelength will be fed back to the gain medium, again passing through the WDM to the port 2 of another three-port circulator (C2) that acted as a mirror by returning all the signal toward the WDM, then to the erbium-doped fiber and the FBG. This repetitive process produced a laser at the FBG reflective wavelength. This output was connected to port 1, which was then emitted at port 2 and traveled to the FBG-FPI of the circulator C1. The reflected light from the FBG-FPI then exited at port 3, connected to a photodetector and a 2.5 G/s 500-MHz oscilloscope.

In the design of the FBG-FPI, these two gratings must be spaced closely together and have the same range of wavelength peak (or at least to be so within ~ 0.1 nm). This is because the sensitivity of the FBG-FPI would be negatively affected if the wavelength of the light source did not match the optimum operating range of the FBG-FPI; indeed, a severe mismatch would render the sensor ineffective. Moreover, as the FBG responds directly to strain and temperature variations, when the surrounding temperature changes, the wavelength shift for the FBG will be identical to that of the FBG-FPI cavity, simultaneously changing the laser wavelength to be always within the FBG-FPI optimum operating range, in that way will offset any temperature change. This feature would enable the sensor to achieve thermal stability where the light source wavelength does not have to be manually tuned when a temperature variation occurs. Finally, a piezoelectric transducer was placed on top of the FBG-FPI, separated by a $20 \times 20 \times 1$ mm plastic sheet as shown in Fig. 3(b), showing a seismic scenario activity occurred will be detected.

The output spectrum obtained from the experimental setup shown in Fig. 3 is shown in Fig. 4, obtained by connecting an optical spectrum analyzer (OSA) to port 3 of the circulator C1 instead of the oscilloscope. As indicated above, the peak (1547.42 nm) is within the optimum operating range of the FBG-FPI (1547.15 to 1547.80 nm).

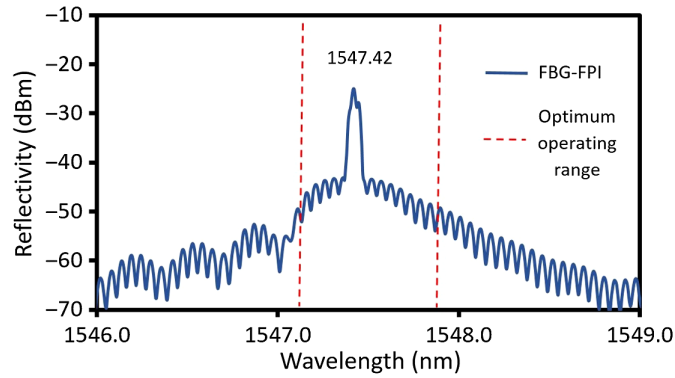


Fig. 4 The output spectrum of FBG and FBG-FPI from port 3 of the circulator when connected to an OSA.

2.4 Burst Signal at Low-Frequency Interval

Regarding Fig. 3(b), a 0.5-V peak-to-peak voltage (V_{pp}) 3-kHz burst signal from the ROHDE and SCHWARZ RTM3004 signal generator (SG) was applied to the FBG-FPI, using a piezoelectric transducer where the frequency of the burst interval was varied from 1, 2, and 3 Hz.

2.5 High Frequency of Sinusoidal Wave

Using the same setup as discussed above, a 3-kHz sine wave with 5 V_{pp} from the SG was applied to the FBG-FPI through the piezoelectric transducer. The input frequency was varied up to 9- in 3-kHz intervals. To allow a cross-comparison, the experiment was repeated using a conventional piezoelectric sensor to compare the performance characteristics of the two approaches used to monitor vibration.

2.6 Temperature Monitoring and Correction for Temperature Effects

The procedures above were carried out by placing the experimental setup on a hot plate to investigate the effect of temperature on the FBG-FPI sensor. Due to the small size of the device shown schematically in Fig. 3, as the wavelength shifts due to the temperature of the FBGs used are the same for each, there should then be no changes in the ability of the FBG-FPI to operate as an interferometer and thus capture the vibration waveforms (generated in this test by the SG at known frequencies). An illustration of the experimental setup used for calibration of the system is shown in Fig. 5, where both the FBGs and the FBG-FPI were placed on top of a hot plate and between the piezoelectric transducers. A thermocouple was utilized in this calibration to monitor the temperature of the hot plate. When it was raised from $\sim 26^{\circ}\text{C}$ to 80°C in 10°C intervals, the wavelength spectrum of the FBG-FPI from port 3 of the circulator C1 was observed and recorded by the OSA. Such calibration is required and a pre-condition for the sensor system in vibration monitoring. The FBG-FPI continues to work well over this temperature range, showing that both gratings' wavelength shift (due to changes in the temperature) is essentially identical (with a sensor of this small size). The burst signals at low frequency and sinusoidal signals at high frequency, as mentioned in Secs. 2.4 and 2.5, were performed from $\sim 26^{\circ}\text{C}$ to 80°C , at 10°C intervals, and the waveforms from FBG-FPI were recorded using an oscilloscope.

3 Results and Discussions

The output signals (generated directly from the SG in the system calibration setup shown in Fig. 3) are shown in Fig. 6. Figure 6(a) shows the 3 kHz burst signal in a 1-s interval (1 Hz), and Fig. 6(b) shows the 3-kHz sine signal. After being exposed to the 3-kHz burst signal, the responses of the FBG-FPI sensor to the burst signal are shown in Fig. 7. This allows a comparison between the output signal of the SG and (what should then be a similar) output signal

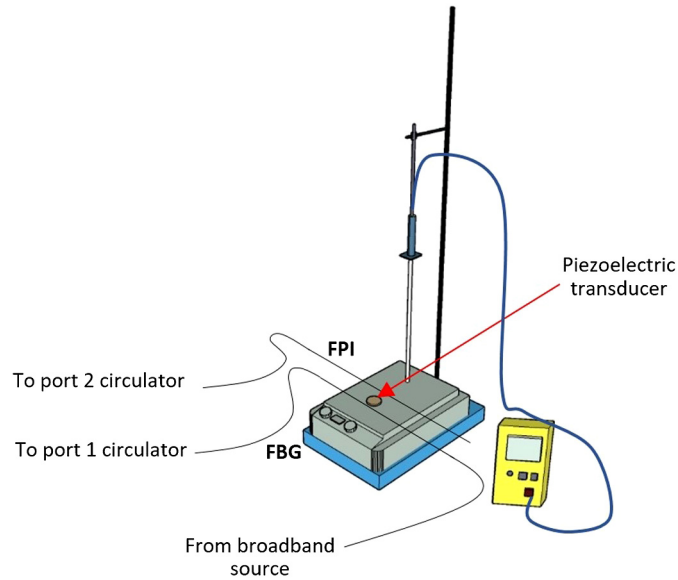


Fig. 5 Experimental setup for the calibration of the FBG-FPI sensor over a wide temperature range, from $\sim 26^{\circ}\text{C}$ to 80°C , at 10°C intervals.

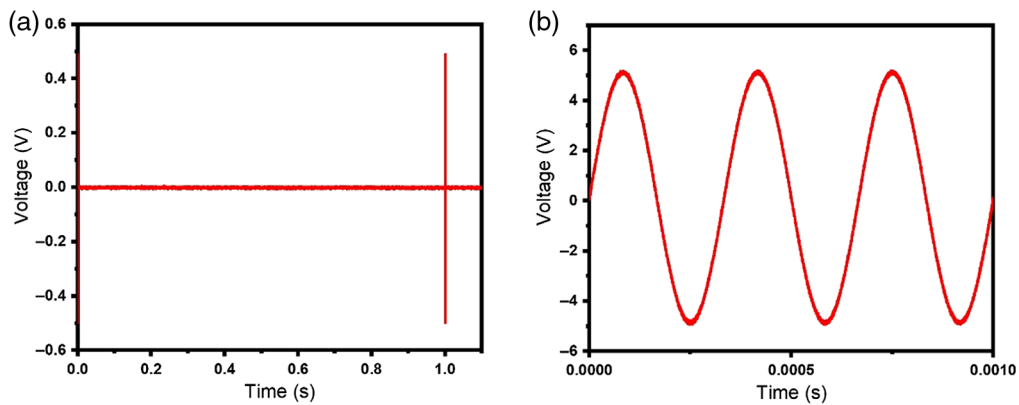


Fig. 6 (a) Signals directly from the SG: 3-kHz burst at a 1-Hz interval and (b) 3-kHz sine wave, generated by the SG.

detected by the FBG-FPI. Figures 7(a)–7(c) show the FBG-FPI response to the 3-kHz burst signal in 1-, 2-, and 3-Hz intervals, respectively.

As shown in Fig. 7, there is minimal background noise in the output reading, primarily due to the suitable nature of the input broadband source.³⁵ Compared to the output obtained directly from the SG (Fig. 6), a small voltage (amplitude) difference between the SG output ($0.5 V_{pp}$) and the FBG-FPI output (~ 0.2 to $0.3 V_{pp}$) is due to the energy loss experienced by the sensor. However, the similarity in the structure of the pulses demonstrates that the FBG-FPI performed well in detecting the burst signals at low-frequency intervals.

Figure 8 showed the response of the piezoelectric sensor compared to the FBG-FPI when both were subjected to the 3-kHz sine wave from the SG. Compared to the 3-kHz output directly from the SG in Fig. 6(b), both sensors record an observable loss in input voltage (as elastic waves lose energy as they travel through a material) where in this case, a plastic sheet divides the sensor and the transducer (the vibration source). The slight distortion is seen in the sine wave of the FBG-FPI output signal [in Fig. 8(b)] seems likely to have been caused by the vibration of the fiber itself—the conventional piezoelectric sensor illustrates the sine wave shape better because the sensor plate was metal (likely aluminum), providing a good response to elastic waves. The data show that the FBG-FPI sensor can detect high-frequency resonance similarly to conventional vibration sensors.

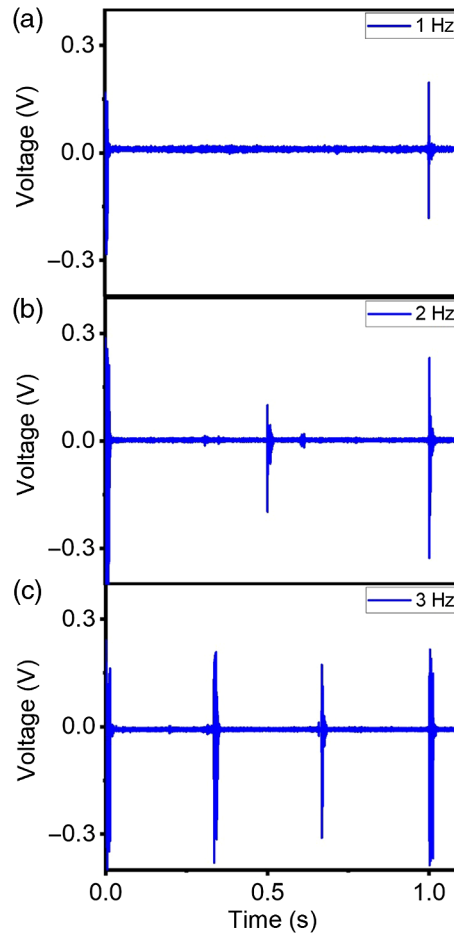


Fig. 7 The comparison between the output signal of the SG and the output signal from the FBG-FPI: 3-kHz burst at (a) 1-, (b) 2-, and (c) 3-Hz intervals detected by the FBG-FPI.

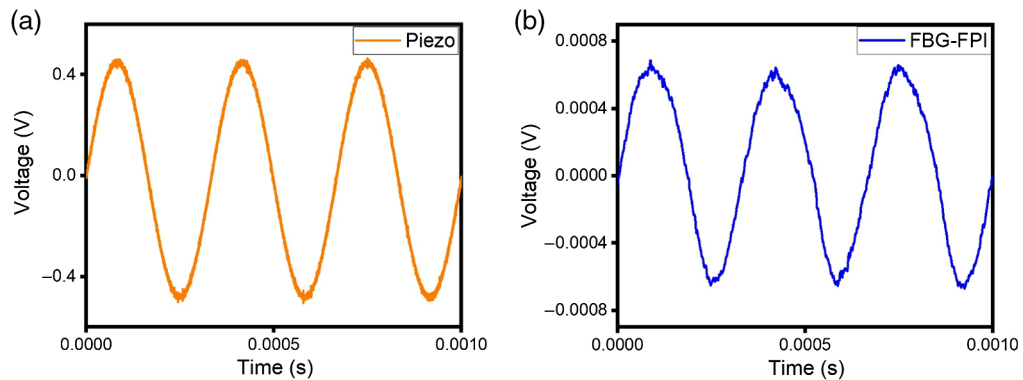


Fig. 8 Output signal detected by (a) the piezoelectric sensor and (b) the FBG-FPI sensor: both were subjected to a similar 3-kHz sine wave.

In addition to the test carried out, where the results are shown in Fig. 8, a comparison was also made between the output signal directly from the SG, the piezoelectric sensor, and the FBG-FPI sensor, as shown in Fig. 9. The results show the output waveform from each sensor when they were subjected to a sinusoidal wave at a series of frequencies of (a) 3, (b) 6, and (c) 9 kHz, where it is evident that FBG-FPI can detect the waveforms at the high-frequency region with high fidelity.

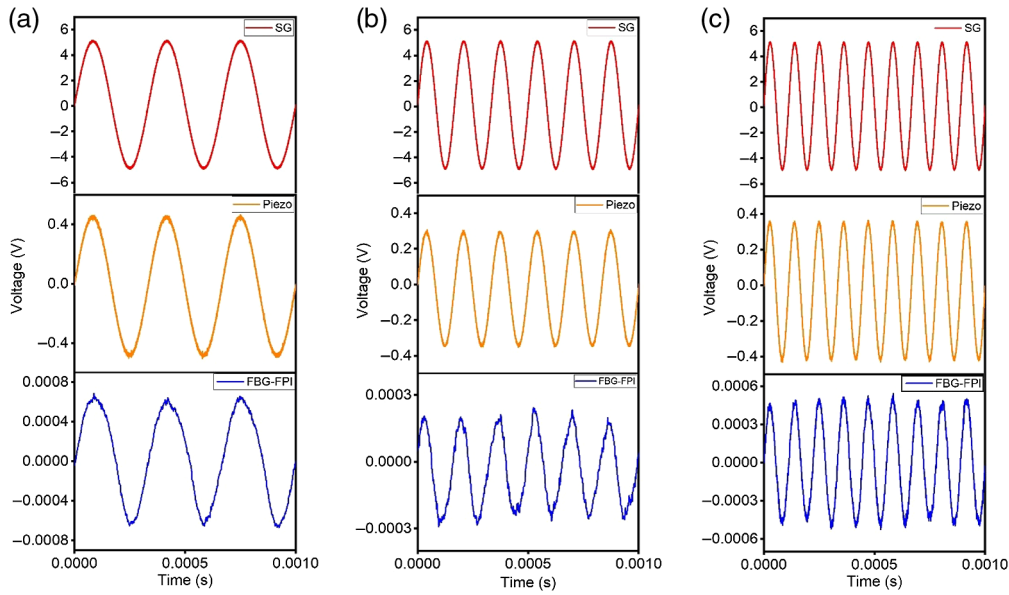


Fig. 9 Output signal comparison between the SG (SG—in red), the piezoelectric sensor (Piezo—in orange), and the FBG-FPI sensor (FBG-FPI in blue) for three different frequencies (a) 3, (b) 6, and (c) 9 kHz.

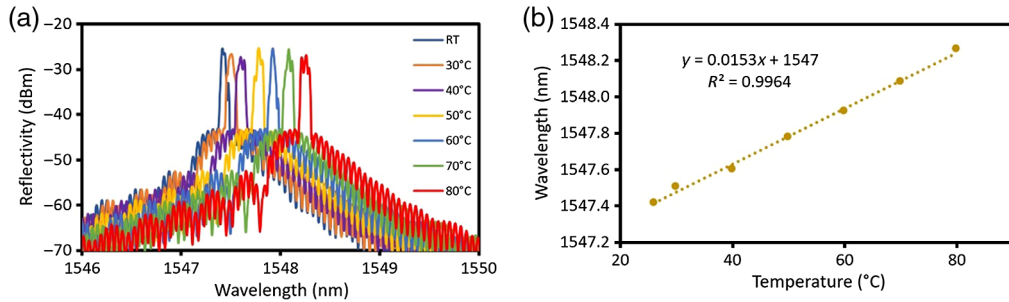


Fig. 10 (a) Output spectra of the FBG-FPI when subjected to different temperatures and (b) the linear response of the FBG-FPI when it is subjected to different temperatures from 26°C to 80°C in 10°C intervals.

The FBG-FPI sensor was subjected to changes in the temperature, over the range from ~26°C (room temperature) to 80°C, to investigate the temperature dependency. To ensure that the temperature parameter can be eliminated as the objective of this work, the output spectra obtained during these tests were recorded at port 3 of the circulator C1 using the OSA, and Fig. 10(a) illustrates the spectra obtained during the temperature rise until 80°C. It can be inferred that the sensor works well across this temperature range as the laser source was always within the optimum operating range of the FBG-FPI (as the FBG and the FBG-FPI were placed closely together, hence, experience temperature changes simultaneously), enabling the FBG-FPI to detect the waveforms regardless of surrounding temperature changes consistently. The linear relationship was obtained for the FBG-FPI output wavelength against the temperature rise, as shown in Fig. 10(b) was used as the calibrated graph. A sensitivity of 0.0153-nm shifts per degree Celsius was obtained from the calibration with an R^2 value of 0.9964, indicating the linear response.

To further validate that the FBG response toward temperature was identical to the FBG-FPI, the spectra for each response of FBG and FBG-FPI toward temperature are shown in Fig. 11(a). The figure shows the spectral responses of both the FBG (top) and the FBG-FPI (bottom) at temperatures of 30°C, 40°C, 50°C, 60°C, 70°C, and 80°C showing that the wavelength shifts of the FBG themselves and that of the FBG-FPI were simultaneous and in tandem when they

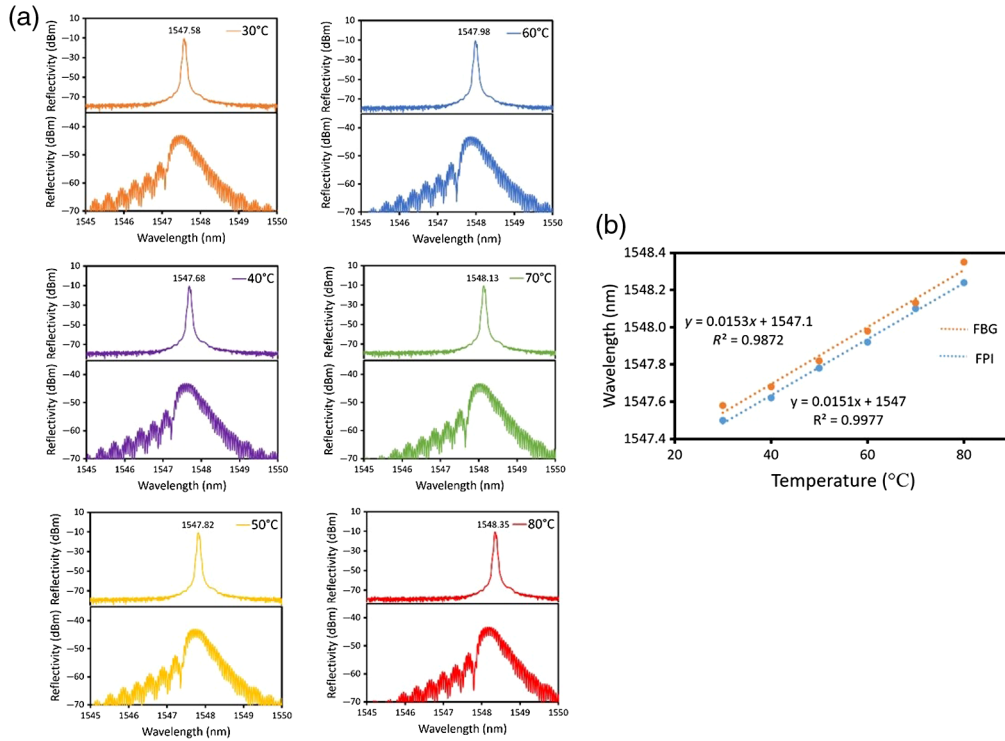


Fig. 11 (a) Response spectra of each FBG and FPI at 30°C, 40°C, 50°C, 60°C, 70°C, and 80°C and (b) the linear relationship for both FBG and FBG-FPI simultaneously when they were subjected to different temperature parameters.

were subjected to the same temperature changes. Figure 11(b) shows the linear response of both FBG and FBG-FPI simultaneously toward temperatures change. The FBG and FBG-FPI shifted linearly, almost identical with 0.0153 nm/°C and 0.0151 nm/°C, respectively. The slight difference of 0.0002 nm/°C is probably due to the grating structure of the FBG and FBG-FPI itself, with FBG-FPI having an interferometric region between the grating. However, this would be insignificant as even at a temperature as high as 80°C, the laser source was still within the optimum operating range of the FBG-FPI, thus indicating that the sensor was sensitive. Thus, Figs. 10 and 11 verify that temperature changes would not affect the ability of the FBG-FPI to detect burst and sine signals, as the laser source is always within the FPI operating range over the temperature excursion range studied.

Figure 12 shows the FBG-FPI responses to a 3-kHz burst at (a) 1, (b) 2, and (c) 3 Hz at room temperature (blue) and 80°C (red). It is clear from Fig. 12(a) that the FBG-FPI can detect the burst signal pattern over all the temperatures in the range shown. Further, similar response patterns can be observed for bursts at 2 and 3 Hz in (b) and (c), respectively. This observation shows that the method proposed can allow the FBG-FPI to detect burst signals at these low frequencies, regardless of the temperature change.

In addition to that, the response of the FBG-FPI to any temperature changes in high-frequency sine waves can be observed in Fig. 13. For example, Fig. 13(a) shows the FBG-FPI can detect the 3-kHz sine waves at temperatures both of 40°C and 80°C, and they exhibit similar responses toward temperature for frequencies of 6 and 9 kHz, as shown in Figs. 13(b) and 13(c), respectively. There is also no observable difference in the amplitude response whenever the FBG-FPI was subjected to different temperatures.

4 Conclusions

This work demonstrates a highly effective FBG-FPI sensor that can detect burst signals at low-frequency intervals of 1, 2, and 3 Hz, as well as sinusoidal waves at the high-frequency region of

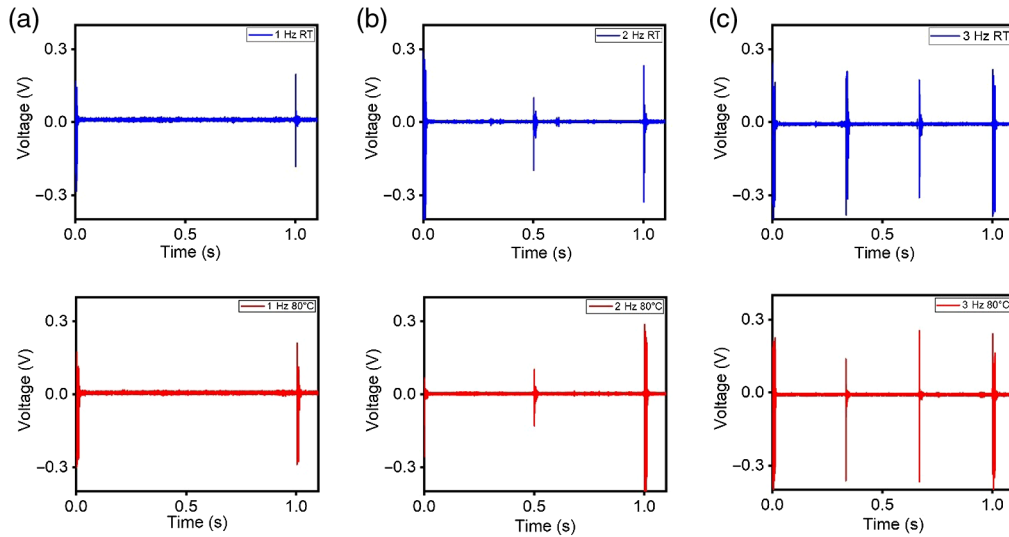


Fig. 12 The response of the FBG-FPI toward 3-kHz bursts at (a) 1-, (b) 2-, and (c) 3-Hz intervals at room temperature (blue) compared to at 80°C (red).

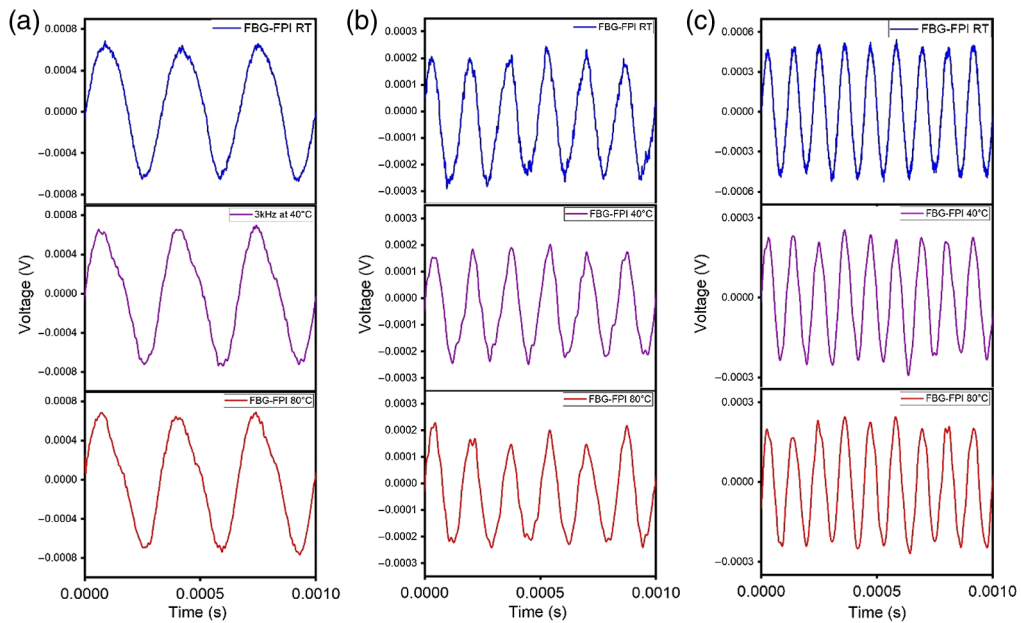


Fig. 13 The response of the FBG-FPI toward (a) 3-, (b) 6-, and (c) 9-kHz sine waves at room temperature (blue), 40°C (purple), and 80°C (red).

3 to 9 kHz. Such frequencies were applied to the sensor to imitate seismic waves present during earthquakes or landslides. From the results shown above, it has been proven that the sensor was effective over the temperature range of 26°C to 80°C and was independent of the temperature changes. This was primarily due to the design where the FBG and the FBG-FPI were placed and aligned closely, causing the light source to always be within the optimum wavelength range to suit the FBG-FPI operating as an interferometer.

Such a small, lightweight, all-optical, and temperature-independent vibration sensor capable of detecting the waveforms of vibration over this frequency range opens up various engineering applications, including SHM and ground movement monitoring others, both particularly important in structural engineering today.

Acknowledgments

The authors are pleased to acknowledge support from the Universiti Malaya (Grant Nos. UM-Innovate PPSI-2020-HICOE-02 and RU005-2021) and also from British Council-MIGHT NUOF (Grant No. IF022-2020). In addition, Grattan acknowledges the support from the Royal Academy of Engineering. The authors declare that they have no known competing financial interests or personal relationships that could have influenced the work reported in this paper.

References

1. A. P. Adewuyi, Z. Wu, and N. H. M. K. Serker, "Assessment of vibration-based damage identification methods using displacement and distributed strain measurements," *Struct. Health Monitor.* **8**(6), 443–461 (2009).
2. Z. Abas et al., "Characterization of electro-active paper vibration sensor by impact testing and random excitation," *Int. J. Appl. Mech.* **7**(4), 1550065 (2015).
3. S. Tadigadapa and K. Mateti, "Piezoelectric MEMS sensors: state-of-the-art and perspectives," *Meas. Sci. Technol.* **20**(9), 092001 (2009).
4. H. C. Lee and W. H. Bae, "Study on the elimination of irreversible magnetic components using anhysteretization in a magnetostrictive vibration sensor," *Trans. Korean Soc. Noise Vibration Eng.* **20**(9), 841–848 (2010).
5. C. T. Chiang, C. I. Chang, and W. Fang, "Design of a digitized vibration detector implemented by CMOS digitized capacitive transducer with in-plane SoI accelerometer," *IEEE Sens. J.* **14**(8), 2546–2556 (2014).
6. X. Liu et al., "Distributed fiber-optic sensors for vibration detection," *Sensors* **16**(8), C1 (2016).
7. P. Kishore et al., "Vibration sensor using 2×2 fiber optic coupler," *Opt. Eng.* **52**(10), 107104 (2013).
8. Z. Zhang and X. Bao, "Continuous and damped vibration detection based on fiber diversity detection sensor by Rayleigh backscattering," *J. Lightwave Technol.* **26**(7), 832–838 (2008).
9. N. Linze et al., "Development of a multi-point polarization-based vibration sensor," *Opt. Express* **21**(5), 5606 (2013).
10. H. Ohno et al., "Industrial applications of the BOTDR optical fiber strain sensor," *Opt. Fiber Technol.* **7**(1), 45–64 (2001).
11. J. Villatoro, V. P. Minkovich, and D. Monzón-Hernández, "Temperature-independent strain sensor made from tapered holey optical fiber," *Opt. Lett.* **31**(3), 305 (2006).
12. A. Masoudi, M. Belal, and T. P. Newson, "A distributed optical fibre dynamic strain sensor based on phase-OTDR," *Meas. Sci. Technol.* **24**(8), 085204 (2013).
13. C. Li et al., "Er³⁺-Yb³⁺ co-doped silicate glass for optical temperature sensor," *Chem. Phys. Lett.* **443**(4–6), 426–429 (2007).
14. A. Irace and G. Breglio, "All-silicon optical temperature sensor based on multi-mode interference," *Opt. Express* **11**(22), 2807 (2003).
15. Z. Zhang and X. Bao, "Distributed optical fiber vibration sensor based on spectrum analysis of polarization-OTDR system," *Opt. Express* **16**(14), 10240 (2008).
16. J. Villatoro et al., "Miniature multicore optical fiber vibration sensor," *Opt. Lett.* **42**(10), 2022 (2017).
17. R. Sifta et al., "Distributed fiber-optic sensor for detection and localization of acoustic vibrations," *Metrol. Meas. Syst.* **22**(1), 111–118 (2015).
18. H. J. Bang, S. M. Jun, and C. G. Kim, "Stabilized interrogation and multiplexing techniques for fibre Bragg grating vibration sensors," *Meas. Sci. Technol.* **16**(3), 813–820 (2005).
19. T. C. Liang and Y. L. Lin, "Ground vibrations detection with fiber optic sensor," *Opt. Commun.* **285**(9), 2363–2367 (2012).
20. L. Lu et al., "Self-mixing signal in Er³⁺-Yb³⁺ codoped distributed Bragg reflector fiber laser for remote sensing applications up to 20 Km," *IEEE Photonics Technol. Lett.* **24**(5), 392–394 (2012).
21. L. Lu et al., "Self-mixing interference in an all-fiberized configuration Er³⁺-Yb³⁺ codoped distributed Bragg reflector laser for vibration measurement," *Curr. Appl. Phys.* **12**(3), 659–662 (2012).

22. C. Wang et al., "Quasi-distributed fiber sensor based on Fresnel-reflection-enhanced Incomplete-POTDR system," *Proc. SPIE* **9634**, 96347F (2015).
23. M. Ren et al., "Theoretical and experimental analysis of Φ -OTDR based on polarization diversity detection," *IEEE Photonics Technol. Lett.* **28**(6), 697–700 (2016).
24. Y. Muanenda et al., "A cost-effective distributed acoustic sensor using a commercial off-the-Shelf DFB laser and direct detection phase-OTDR," *IEEE Photonics J.* **8**(1), 1–10 (2016).
25. Q. Zhang et al., "All-fiber vibration sensor based on a Fabry–Perot interferometer and a microstructure beam," *J. Opt. Soc. Am. B* **30**(5), 1211 (2013).
26. N. Sathitanon and S. Pullteap, "A fiber optic interferometric sensor for dynamic measurement," *Int. J. Mech. Mechatron. Eng.* **1**(11), 667–670 (2007).
27. G. Giuliani et al., "Laser diode self-mixing technique for sensing applications," *J. Opt. A Pure Appl. Opt.* **4**(6), S283 (2002).
28. A. Chijioke and J. Lawall, "Laser Doppler vibrometer employing active frequency feedback," *Appl. Opt.* **47**(27), 4952–4958 (2008).
29. P. Castellini, M. Martarelli, and E. P. Tomasini, "Laser Doppler vibrometry: development of advanced solutions answering to technology's needs," *Mech. Syst. Sig. Process.* **20**(6), 1265–1285 (2006).
30. H. F. Lima et al., "Structural health monitoring of the church of santa casa da misericórdia of Aveiro using FBG sensors," *IEEE Sens. J.* **8**(7), 1236–1242 (2008).
31. U. Tiwari et al., "Health monitoring of steel and concrete structures using fibre Bragg grating sensors," *Curr. Sci.* **97**(11), 1539–1542 (2009).
32. A. Wada, S. Tanaka, and N. Takahashi, "High-sensitivity vibration sensing using in-fiber Fabry–Perot interferometer with fiber-Bragg-grating reflectors," *Proc. SPIE* **7503**, 75033L (2009).
33. A. Wada, S. Tanaka, and N. Takahashi, "Optical fiber vibration sensor using FBG Fabry–Perot interferometer with wavelength scanning and Fourier analysis," *IEEE Sens. J.* **12**(1), 225–229 (2012).
34. Y. J. Rao et al., "Simultaneous strain, temperature and vibration measurement using a multiplexed in-fibre-Bragg-grating/fibre-Fabry–Perot sensor system," *Electron. Lett.* **33**(24), 2063–2064 (1997).
35. M. K. A. Zaini et al., "In-fiber Fabry Perot interferometer with narrow interference fringes for enhanced sensitivity in elastic wave detection," *Opt. Fiber Technol.* **53**, 102021 (2019).

Muhammad Syamil Mohd Sa'ad received his bachelor of science (Hons) degree in pure physics from the Faculty of Science, University of Malaya, in 2019. He is currently a postgraduate student and a research assistant at the Photonics Research Centre, University of Malaya. His research interest focuses on fiber optic sensors mainly on FBG.

Mohammad Faizal Ismail received his bachelor of engineering degree (telecommunication) and master of engineering degree (science) from the Faculty of Engineering, University of Malaya, in 1999 and 2004, respectively. He received his PhD from the same university in 2021, where his research focuses on pulsed, multiwavelength fiber lasers, and waveguides.

Muhammad Khairol Annuar Zaini received his bachelor degree from the Department of Physics, Faculty of Science, University Putra Malaysia, Malaysia, in 2015, followed by a PhD from the University of Malaya. His current research interest includes FBG sensors and spatial division multiplexing.

Kenneth T. V. Grattan received his BSc degree (first class honors) in physics from Queen's University Belfast in 1974, followed by a PhD in laser physics. He received his doctor of science degree from City University in 1992 for his sensor work. His research interests have expanded to include the development and use of fiber optic and optical systems in the measurement of a range of physical and chemical parameters.

B. M. Azizur Rahman received his BSc Eng and MSc Eng degrees in electrical engineering with distinctions from Bangladesh University of Engineering and Technology (BUET), Dhaka, Bangladesh, in 1976 and 1979, respectively. He received his PhD in electronic engineering from

the University College, London in 1982. At City University, he leads the research group on photonics modeling.

Gilberto Brambilla is a professor at the Optoelectronics Research Centre and co-director and general manager of the Future Photonics Hub. He received his MSc degree (engineering) with honors from Politecnico di Milano (Italy) in 1996 and his PhD in optoelectronics from the University of Southampton in 2002. His research interests include optical fiber sensors, optical fiber structuring using fs lasers, specialty and polymer fibers, new fiber fabrication technologies, and fibers for nuclear sensing.

Lim Kok Sing received his BE degree from the Department of Electrical Engineering, Faculty of Engineering, Universiti Malaya, Malaysia, in 2008, and received his PhD from the Photonics Research Centre, Universiti Malaya in 2012. He is currently a senior lecturer at the Photonics Research Centre, University of Malaya. He is a corporate member of the Institute of Engineers Malaysia (IEM), a registered professional engineer (telecommunication) of the Board of Engineers Malaysia, and a member of OSA.

Harith Ahmad received his PhD in laser technology from the University of Wales, Swansea, United Kingdom, in 1983. He is currently a professor in the Department of Physics and a director at the Photonics Research Center, Universiti Malaya, where he has actively pursued research activities in the field of photonics since 1983. He has authored more than 400 professional papers in international journals and conferences. His research interests are in lasers, fiber-based devices for telecommunications, and fiber-based sensor devices.